IEEE Photonics Journal
An IEEE Photonics Society Publication

Open Access

A Real-Time Restraint Method for Range Walk Error in 3-D Imaging Lidar Via Dual Detection

Volume 10, Number 2, April 2018

Ling Ye
Guohua Gu
Weiji He
Huidong Dai
Qian Chen

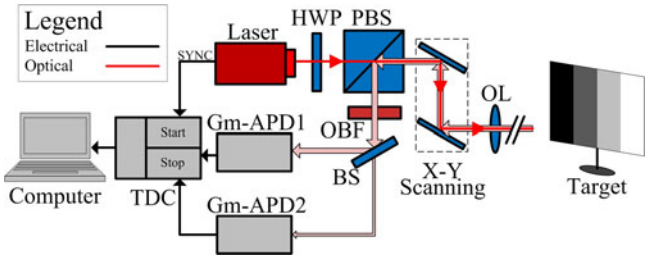

DOI: 10.1109/JPHOT.2018.2816652
1943-0655 © 2018 IEEE

IEEE photonics SOCIETY

IEEE

A Real-Time Restraint Method for Range Walk Error in 3-D Imaging Lidar Via Dual Detection

Ling Ye,[1] **Guohua Gu**,[1] **Weiji He**,[1,2] **Huidong Dai**,[1] **and Qian Chen**[1]

[1] Jiangsu Key Laboratory of Spectral Imaging & Intelligence Sense, Nanjing University of Science and Technology, Nanjing 210094, China
[2] Key Laboratory of Intelligent Perception and Systems for High-Dimensional Information of Ministry of Education, Nanjing University of Science and Technology, Nanjing 210094, China

DOI:10.1109/JPHOT.2018.2816652

Manuscript received November 14, 2017; revised March 3, 2018; accepted March 13, 2018. Date of publication March 16, 2018; date of current version March 29, 2018. This work was supported in part by the Seventh Six-talent Peak project of Jiangsu Province under Grant 2014-DZXX-007, in part by the National Natural Science Foundation of China under Grant 61271332, in part by the Fundamental Research Funds for the Central Universities under Grant 30920140112012, in part by the Innovation Fund Project for Key Laboratory of Intelligent Perception and Systems for High-Dimensional Information of Ministry of Education under Grant JYC01509, and in part by the Fund Project for Low-light-level Night Vision Laboratory under Grant J20130501. Corresponding author: Guohua Gu (e-mail: gghnjust@163.com).

Abstract: Geiger-mode avalanche photodiode (Gm-APD) offers 3D imaging lidar much better capability in terms of detection sensitivity. However, a range walk error (RWE) exists in Gm-APDs which refers to the fluctuation of the measured distance as a function of the intensity of echo pulses. In this paper, we present a real-time restraint method for RWE implemented by unequally intensity-dividing the echo pulses into two Gm-APDs. The difference image of two depth images measured by the divided beams is a matrix of RWE distribution and the intensity image is used to censor the anomalous pixels in the matrix. Combined with the matrix of RWE distribution, an accurate depth image with low RWE can be obtained. Experimental results demonstrate that the proposed method reduces approximately 86% RWE of the conventional method in real time.

Index Terms: Lidar, photon counting, three-dimensional imaging, range walk error.

1. Introduction

3D imaging lidar illuminates targets by laser pulses and exploits the back-reflected optical flux to acquire depth information and reflectivity of the scene [1]–[8]. Geiger-mode avalanche photodiode (Gm-APD), which has ultrahigh sensitivity and high-resolution timing, is widely used with the technique of time-correlated single-photon counting (TCSPC) in lidar systems to detect the weak echo-pulse in low-light-level environments [9], [10]. McCarthy *et al.* reported their scanning lidar system which achieves sub-pulse depth-resolution in a range of a kilometer [11]–[13]. Altmann *et al*. of the same research group in Heriot-Watt University proposed new Bayesian algorithms to reconstruct depth images using sparse single-photon data [14], [15]. Kirmani *et al*. recently proposed a method which only used first photon detected in each pixel to recover 3D structure and

reflectivity of the scene [16]. This method is valuable in fields with few back-reflected photons such as microscopy and remote sensing.

Because of the existence of the inevitable noise, including the dark count noise, background noise and so on, ultrahigh sensitivity of Gm-APDs brings significant challenges to obtain a clear depth image of targets. Kong *et al.* proposed a method that the intensity of the echo laser pulse was equally divided into two Gm-APDs and then the electrical signals from the two Gm-APDs were compared by an AND gate to filter the noise [17]. Their method greatly reduced the false alarm compared with the single Gm-APD method. Similarly, Zhang *et al*. presented a real-time denoising method using 3×3 Gm-APDs. According to the continuity of the surfaces of most targets, nine adjacent pixels were taken as one elementary unit and the total logic level of the nine pixels of one elementary unit was used to distinguish signal and noise compared with a threshold [18].

Besides, Gm-APDs have an intrinsic property that the temporal peak position is as a function of count rate. This property leads to an error named range walk error (RWE) which is fluctuated with the intensity of back-reflected laser pulse. In practical measurement, the reflectivity of targets is unknown and has a great varying range so the RWE is hard to expectable. Rech *et al*. made a progress in the aspect of Gm-APDs' circuit. They added an additional timing circuit board in a Gm-APD to reduce the RWE and timing jitter [19] and Warburton *et al*. utilized this modification to achieve a surface separation resolution as low as 1.7 cm [20]. Oh *et al*. proposed a method which used a theoretical model based on Poisson statistics and two measurements to reduce the RWE [21]. Xu *et al*. presented a recursive method to obtain the signal photoelectron distribution and used Gaussian functions fitting method to fit a curve to restrain the RWE [22]. Researchers of our group used a priori modeling based on the relationship between the RWE and the response rate of emitting pulses to correct the RWE in practical measurement [23]. It required manual intervention to build the priori modeling. Time consuming and errors along with it would restrict the application of this method.

In this paper, we propose a more universal method to reduce the RWE by dividing the intensity of echo-pulse unequally into two Gm-APDs; the low intensity beam is used to reduce the RWE of the strong beam. Without a priori modeling or amounts of post-processing, our method is able to reduce the RWE in real time.

2. RWE Reduction Method

The echo pulse is unequally divided into a weak part and a strong part in our method. The weak part is used to obtain the RWE distribution as a reference beam. Then the correlation between RWE and intensity of echo pulse is exploited to improve the accuracy of the RWE distribution. Finally, the depth image obtained from the strong part reduces RWE combined with RWE distribution. The detailed procedures are illustrated as Fig. 1: Laser pulses are transmitted to the target and then the received back-reflected pulses are intensity-divided into two beams at unequal ratio (10% and 90% for an example in this paper). Gm-APDs and TCSPC are used to detect the echo pulses and obtain the distribution histogram. As same as conventional imaging lidar, an intensity image (a) and a depth image with RWE (b) of the target are obtained based on the strong beam. Due to the low intensity of the weak beam, a rough depth image with low RWE (c) is obtained, where some pixels have few photons even no photons detected to do anomalous detections, called damaged pixels. A matrix of RWE distribution (d) is acquired by subtracted the two depth images (b) and (c). Meanwhile, the matrix of RWE distribution (d) inherits the damaged pixels from the rough depth image (c). In order to censor and repair the damaged pixels, the intensity image (a) is exploited to find pixels which have the same intensity as the damaged pixel because RWE is a function of the intensity of echo pulses. Hence, the damaged pixels are given data from pixels which have the same intensity in (a) and then the matrix of RWE distribution without damaged pixels (e) is obtained. Base on (e), a correction of RWE can be implemented on (b) to acquire a depth image with low RWE (f). Finally, we can obtain an accurate depth-intensity image (g) by combining (a) with (f).

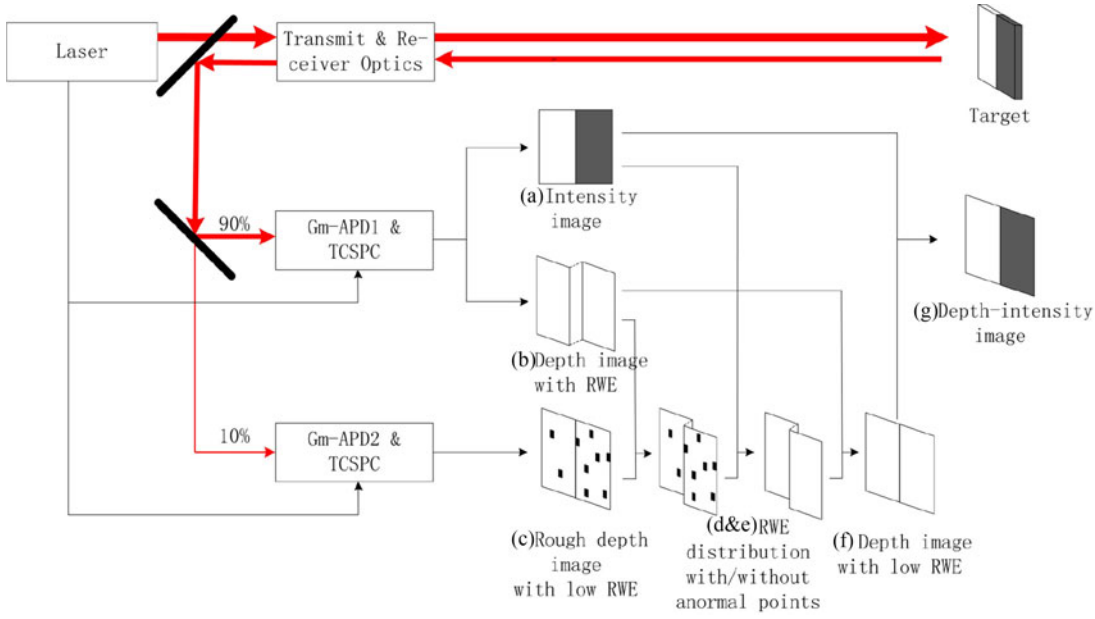

Fig. 1. Schematic diagram of the proposed RWE reduction method.

3. Theoretical Analysis

For normal Q-switched laser, the temporal distribution of primary electrons generated by the echo pulse, $S_{PE}(t)$ is given by [24],

$$S_{PE}(t) = \frac{S_{PE\_tot}}{\tau}\frac{t-\tau_d}{\tau}\exp\left(-\frac{t-\tau_d}{\tau}\right) \tag{1}$$

where τ is a parameter related to pulse width of the emitting laser pulse, $p_w = 3.5\tau$; τ_d is the round-trip time of the laser pulse; S_{PE_tot} is total number of the primary electrons generated by an echo laser pulse and is given by [17], [25],

$$S_{PE\_tot} = \frac{\eta_q \lambda}{hc} E_T \left(\frac{FOV}{\theta_T}\right)^2 \frac{\rho}{\pi}\cos\theta_{\text{target}}\frac{A_R}{R^2}\eta_{EC}\eta_T\eta_R\eta_A^2 \tag{2}$$

According to the devices used in the system, the definitions of the parameters along with values selected for illustration are follows: the quantum efficiency η_q is 0.46; the wavelength of emitting laser, λ, is 830 nm; the Planck constant h times the speed of light c is 2×10^{-25}Jm; E_T is the energy of an emitting laser pulse; the field of view of the receiver, FOV, is 0.2 mrad; the divergence angle of the emitting laser θ_T is 0.4 mrad; assuming the target is Lambertian, the reflectivity of the target ρ is 0.99; the angle of incidence of the emitting laser, θ_{target}, is 0rad; the area of receiver A_R is π(30 mm)^2; the distance apart from the target R is 20 m; the fraction of the encircled energy falling in the active area of the detector η_{EC} is 0.2; the transmissions of the transmitter optics η_T, the receiver optics η_R and the atmosphere η_A are 0.6, 0.3, 1, respectively. During one measurement using the same system, S_{PE_tot} can be consider proportional to the reflectance of target and when the detection number is large enough the intensity information of pixel (i, j) can be obtained by

$$I(i,j) = \frac{CNT_D(i,j)}{CNT_E} \tag{3}$$

where $CNT_D(i, j)$ is the detection number in pixel (i, j) and CNT_E is the total number of emitting laser pulses during the dwell time of each pixel.

According to the response model of Gm-APD based on the Poisson statistics, the detection probability on the i-th time bin, $P_{D\_bin}(i)$, is given by [10], [25]

$$P_{D\_bin}(i) = \exp\left[-(i-1)\tau_{bin}N_{PE} - \int_0^{(i-1)\tau_{bin}} S_{PE}(t)\,dt\right] \times \left\{1 - \exp\left[-\tau_{bin}N_{PE} - \int_{(i-1)\tau_{bin}}^{i\tau_{bin}} S_{PE}(t)\,dt\right]\right\} \quad (4)$$

where τ_{bin} is the time duration of a time-bin which corresponds to timing resolution of TCSPC; N_{PE} is the average noise count of firing cases in a time-bin, which is from background noise (N_{BG}) and dark count (N_{Dark}). In this paper, for simplification, N_{BG} and N_{Dark} is assumed to be constant. In the case of dual Gm-APD with intensity dividing at a rate of 1/9, the detection probabilities are

$$P_{D\_bin\_10\%}(i) = \exp\left[-(i-1)\tau_{bin}(N_{Dark} + 0.1N_{BG}) - \int_0^{(i-1)\tau_{bin}} 0.1S_{PE}(t)\,dt\right] \times \left\{1 - \exp\left[-\tau_{bin}(N_{Dark} + 0.1N_{BG}) - \int_{(i-1)\tau_{bin}}^{i\tau_{bin}} 0.1S_{PE}(t)\,dt\right]\right\} \quad (5)$$

$$P_{D\_bin\_90\%}(i) = \exp\left[-(i-1)\tau_{bin}(N_{Dark} + 0.9N_{BG}) - \int_0^{(i-1)\tau_{bin}} 0.9S_{PE}(t)\,dt\right] \times \left\{1 - \exp\left[-\tau_{bin}(N_{Dark} + 0.9N_{BG}) - \int_{(i-1)\tau_{bin}}^{i\tau_{bin}} 0.9S_{PE}(t)\,dt\right]\right\} \quad (6)$$

According to [10], the total detection probability during a gating time, $P_D = \sum P_{D\_bin}(i)$, mainly varies in the range of $0.1 \le S_{PE\_tot} \le 10$ and the theoretical analysis will be under this condition. Using the center of mass detection method, the flight time of the laser pulse, $\tau_{TOF}(S_{PE\_tot})$, can be obtained by

$$\tau_{TOF}(S_{PE\_tot}) = \frac{\sum_{i=1}^{N} P_{D\_bin}(i) i\tau_{bin}}{\sum_{i=1}^{N} P_{D\_bin}(i)} \quad (7)$$

The RWE is defined by

$$RWE = \frac{c}{2} \times [\tau_{TOF}(S_{PE\_tot}) - \tau_0] \quad (8)$$

where τ_0 is the reference value of τ_{TOF} without RWE. Here we assume that $\tau_0 = \tau_{TOF}(S_{PE\_tot} = 0.1)$ because when $S_{PE\_tot} \le 0.1$ the echo pulse is weak and RWE can be negligible.

According to (5)–(8), the RWEs of 10% and 90% intensity of the echo pulse are given by

$$RWE_{10\%} = \frac{c}{2} \times \left[\frac{\sum_{i=1}^{N} P_{D\_bin\_10\%}(i) i\tau_{bin}}{\sum_{i=1}^{N} P_{D\_bin\_10\%}(i)} - \tau_0\right] \quad (9)$$

$$RWE_{90\%} = \frac{c}{2} \times \left[\frac{\sum_{i=1}^{N} P_{D\_bin\_90\%}(i) i\tau_{bin}}{\sum_{i=1}^{N} P_{D\_bin\_90\%}(i)} - \tau_0\right] \quad (10)$$

Fig. 2 shows how RWEs and detection probabilities vary with S_{PE_tot} increasing according to (1)–(10). RWE of undivided echo pulse and $RWE_{90\%}$ increase slowly within $0.1 \le S_{PE\_tot} \le 1$ and have a sharp rising edge when $S_{PE\_tot} \ge 1$. The idea behind our strategy is to spread $RWE_{90\%}$ from $0.1 \le S_{PE\_tot} \le 1$ to $0.1 \le S_{PE\_tot} \le 10$, as the dash box and the arrow shown. This avoids the rapid growth of RWE within $1 \le S_{PE\_tot} \le 10$.

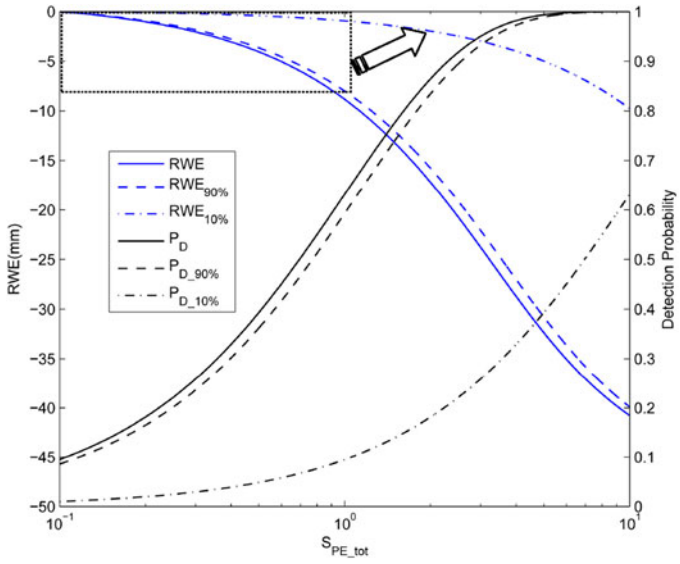

Fig. 2. RWEs and detection probabilities of different intensity-divided rates versus the energy of echo pulse.

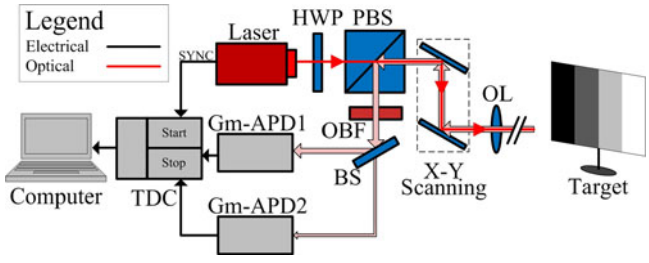

Fig. 3. The schematic diagram of the experimental system. BS, 10:90 beam splitter; OL, objective lens; SYNC, synchronous trigger of the laser source.

However, low intensity brings low RWE while it also reduces the detection probability. This leads to damaged pixels in the matrix of RWE distribution as mentioned above. Some damaged pixels derive from anomalous detections because of low flux and influence of noise. These damaged pixels in the matrix of RWE distribution can be distinguished and given data by the median filter computed by the values of RWE of eight pixels which have same intensity. The other damaged pixels cannot be given data because all of the pixels which have the same intensity have no detections. For example, when $S_{PE\_tot} \rightarrow 0.1$, the detection probability of the 10% intensity of echo pulse in Gm-APD2, $P_{D\_10\%}$ trends toward to 0 and is too low to be detected. Meanwhile, RWE of the 90% intensity of the echo pulse is low so it can be negligible. So RWE of these pixels is considered to be zero. After repairing the damaged pixels, the proposed method approaches a high detection probability as the 90% intensity echo pulse and low RWE as the 10% intensity echo pulse.

4. Experimental Result and Result

Fig. 3 shows the experimental system of the proposed method. An 830-nm laser source (Pico-Quant GmbH, PDL800-B, width of laser pulse 300 ps) is adopted to emit laser pulses to a coaxial transceiving system at a repetition frequency of 2.5 MHz. After passing through a half-wave plate

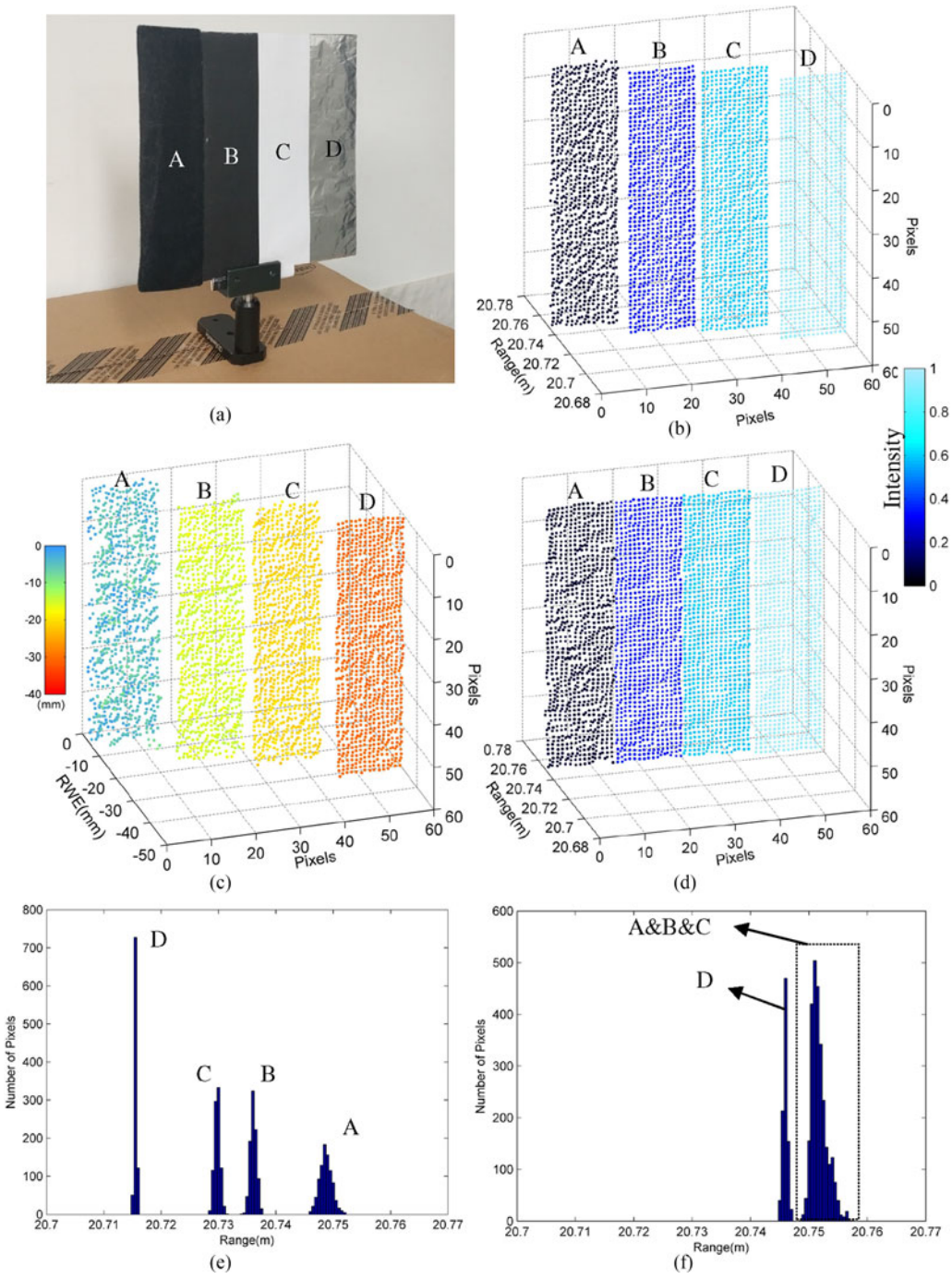

Fig. 4. (a) Photograph of the target. (b) Depth-intensity image of conventional method. (c) Repaired matrix of RWE distribution. (d) Intensity-depth image of the proposed method. (e), (f) Range histograms of conventional and proposed method.

(HWP), the direction of the transmitted laser pulses is controlled by a polarization beam splitter (PBS). Then a 2-axis scanning galvo system is used to direct the transmitted laser pulse to scan the scene of interest in a raster-scanned manner.

An optical bandpass-filter (OBF) with 55% peak transmittance at 830 nm is used to reduce the background noise in the back-reflected optical flux. Then the echo pulses are intensity-divided

into two beams in unequal ratio of 10:90 through a plate beam splitter and coupled into two Gm-APDs (PerkinElmer, SPCM-AQR-14) through fibers respectively. The two Gm-APDs have been calibrated by measuring the same target in the same lidar system and the differences between the results of the two Gm-APDs can be ignored considering the timing jitter of the entire experimental setup. The Gm-APDs have a dead time of 50 ns, a timing jitter of 350 ps and mean dark-count frequency of 50 Hz. The output of the Gm-APDs triggers the time-to-digital converter (TDC) (Agilent U1051A, 6 channels, time resolution 50 ps) to record the time-of-fight (TOF) which begins with the synchronizing signal offered by the laser source. Finally, the depth image of the target is obtained by the TOF information of echo pulse. The measurement time of each scanning point is set to 10 ms. The noise photoelectron is measured by turning off the laser source, which is about 9 kHz.

Fig. 4(a) shows the target consisting of 4 same width zones (A, B, C and D, from left to right) with different reflection rates at ∼20 m from the experimental system and at the distance the target can be considered a flat plate. From left to right, the reflection rates of the four different materials are ascending. The depth image of conventional method using one Gm-APD has severe RWE among different zones as shown in Fig. 4(b). As can be seen, the right zone has smaller depth value and the RWE of zone D which has the highest reflectivity is up to 35 mm on the basis of far left zone A. Under the same condition, the proposed method is employed to restraint the RWE and the experimental result are shown in Fig. 4(c) and (d). Combined with the repaired matrix of RWE distribution, the final depth image of the proposed method significantly reduces the RWE to about 5 mm and is very close to the real target. The histograms of depth distribution of Fig. 4(b) and (d) are shown in Fig. 4(e) and (f), respectively. The depth distribution is separated to 4 parts because of the RWE as shown in Fig. 4(e). However, as presented in Fig. 4(f), the depth values obtained by the proposed method cluster together and have much lower standard deviation. It illuminates the proposed method reduces the impact of RWE which will bring different distortion in depth values because of the fluctuation of intensity of the echo pulses and makes depth values approach to the actual distribution. Meanwhile, without prior modeling and amounts of post-processing, the consumed time of the proposed method has little increment than conventional method so RWE is restrained effectively in real time. Additionally, the depth values in Fig. 4(f) are not integrated into one part completely and there is a small interval between the histograms of zone D and the three other zones. Because the reflectance of zone D is quite high ($S_{PE\_tot} \sim 10$) and the echo pulse with 10% intensity in Gm-APD2 still brings a small amount of RWE. For most application fields ($0.1 \leq S_{PE\_tot} \leq 10$), two-level dividing (0.1/0.9) of the proposed method approaches the balance of efficiency and complexity. As for the special case of high dynamic range, the multiple intensity-dividing, such as 0.01/0.09/0.9, can be considered to deal with it.

The standard deviation of the depth image is given by

$$\sigma = \sqrt{\frac{1}{N-1}\sum_{i=1}^{N}\left(R_{i,j} - \overline{R}\right)^2}$$

where N is the total number of pixels in the depth image; $R_{i,j}$ is the measured distance of the pixel at *i*-th line *j*-th column; $\overline{R}$ is the average measured depth value. The standard deviation of the depth image using conventional method is 14.2 mm while the standard deviation of the proposed method is reduced to 2.8 mm.

The experimental results of a natural scene-a china cup surrounded by a thin silicone loop and a small football-are shown in Fig. 5. The silicone zone of the cup and the black zone of the football have much lower reflectance than the other part. Fig. 5(c) shows that the results of conventional method suffer from depth distortion brought by the RWE in zones which have same depth but large fluctuations of reflectance, such as the silicone zone of the cup and the black zone of the football. Using the proposed method, the RWE is observably reduced as shown in Fig. 5(d).

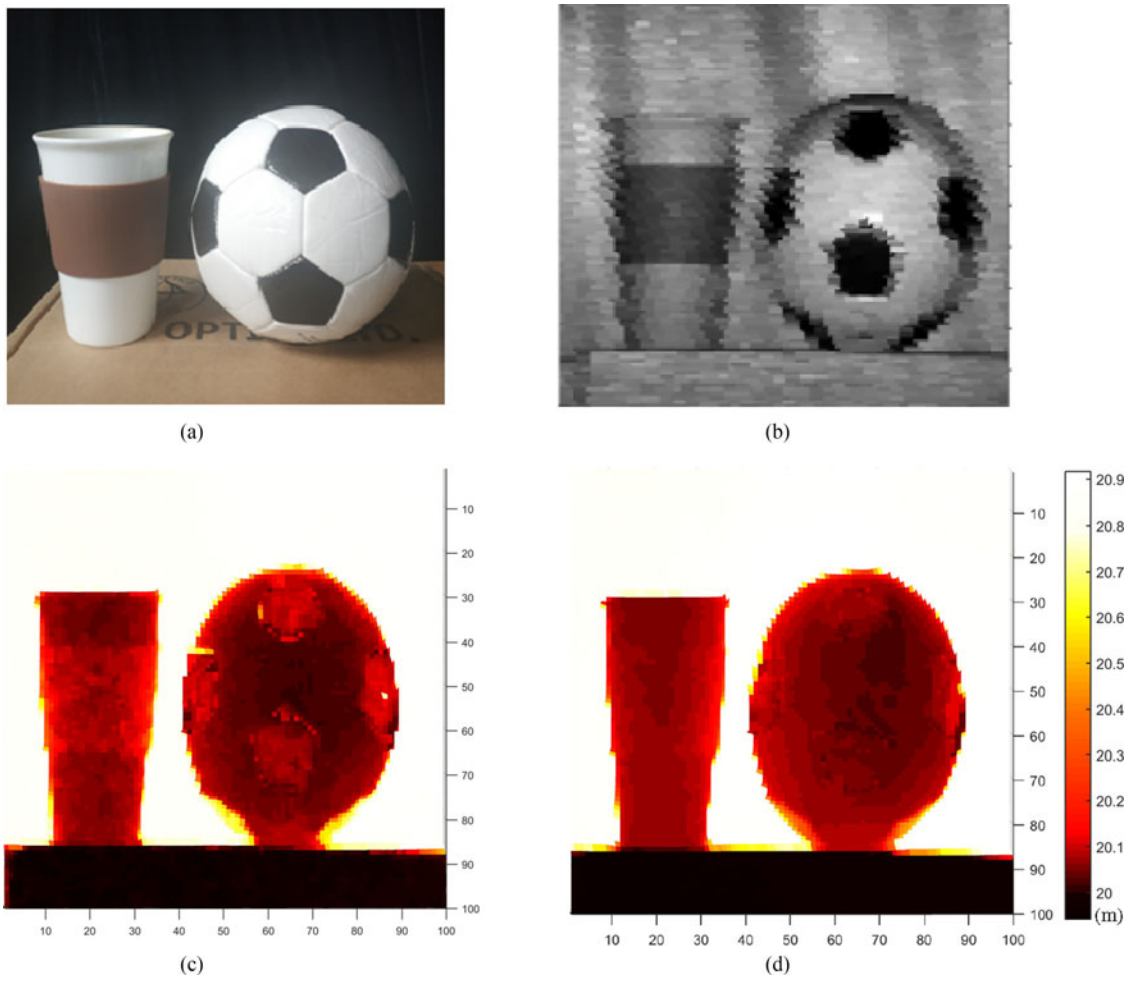

Fig. 5. (a) Photograph of the targets. (b) Intensity image of the targets. (c) Depth image of the conventional method (d) Depth image of the proposed method.

5. Conclusion

In this paper, a RWE-restraint approach without prior modeling is proposed. The method is implemented by dividing the intensity of echo-pulse unequally into two Gm-APDs. Then subtracting the two depth images generated by the divided beams, a matrix of RWE distribution is obtained. Exploiting the correlation between RWE and intensity of echo pulses, the anomalous value in the matrix of RWE distribution is repaired. Finally, combined with the repaired matrix of RWE distribution, the depth image obtained by stronger beam in Gm-APD1 significantly restrains RWE caused by high intensity of echo pulses. Even though two Gm-APDs are needed, the proposed method realizes a real-time restraint of RWE. Different from methods which estimate RWE from photon data with high RWE, the existence of 10% arm saves photon data with low RWE contributed to depth profile and avoids time-consuming and distortion brought by prior modeling and curve fitting. For the designed target of the flat plate, RWE decreases from 35 mm to 5 mm using the proposed method in real time. For the natural scene, the distortion produced by RWE is significant suppressed by the proposed method. The proposed method may be valuable to applications that need fast 3D imaging, such as military reconnaissance and remote sensing.

Reference

[1] W. C. Priedhorsky, R. C. Smith, and C. Ho, "Laser ranging and mapping with a photon-counting detector," *Appl. Opt.*, vol. 35, no. 3, pp. 441–452, 1996.
[2] B. Schwarz, "Mapping the world in 3D," *Nat. Photon.*, vol. 4, no. 7, pp. 429–430, 2010.
[3] R. M. Marino and W. R. Davis, "Jigsaw: A foliage-penetrating 3D imaging laser radar system," *Lincoln Lab. J.*, vol. 15, no. 1, pp. 23–36, 2005.
[4] B. F. Aull *et al.*, "Geiger-mode avalanche photodiodes for three-dimensional imaging," *Lincoln Lab. J.*, vol. 13, no. 2, pp. 335–349, 2002.
[5] M. A. Albota *et al.*, "Three-dimensional imaging laser radars with Geiger-mode avalanche photodiode arrays," *Lincoln Lab. J.*, vol. 13, no. 2, pp. 351–370, 2002.
[6] U. C. Herzfeld *et al.*, "Algorithm for detection of ground and canopy cover in micropulse photon-counting lidar altimeter data in preparation for the ICESat-2 mission," *IEEE Trans. Geosci. Remote Sens.*, vol. 52, no. 4, pp. 2109–2125, Apr. 2014.
[7] P. R. Barbosa, "Remapping the world in 3D," *IEEE Potentials*, vol. 29, no. 2, pp. 21–25, Mar./Apr. 2010.
[8] D. Shin, A. Kirmani, V. K. Goyal, and J. H. Shapiro, "Photon-efficient computational 3-D and reflectivity imaging with single-photon detectors," *IEEE Trans. Comput. Imag.*, vol. 1, no. 2, pp. 112–125, Jun. 2015.
[9] J. S. Massa, A. M. Wallace, G. S. Buller, S. J. Fancey, and A. C. Walker, "Laser depth measurement based on time-correlated single-photon counting," *Opt. Lett.*, vol. 22, no. 8, pp. 543–545, 1997.
[10] D. G. Fouche, "Detection and false-alarm probabilities for laser radars that use Geiger-mode detectors," *Appl. Opt.*, vol. 42, no. 27, pp. 5388–5398, 2003.
[11] A. McCarthy, R. J. Collins, N. J. Krichel, V. Fernández, A. M. Wallace, and G. S. Buller, "Long-range time-of-flight scanning sensor based on high-speed time-correlated single-photon counting," *Appl. Opt.*, vol. 48, no. 32, pp. 6241–6251, 2009.
[12] A. McCarthy *et al.*, "Kilometer-range depth imaging at 1550 nm wavelength using an InGaAs/InP single-photon avalanche diode detector," *Opt. Exp.*, vol. 21, no. 19, pp. 22098–22113, 2013.
[13] A. McCarthy *et al.*, "Kilometer-range, high resolution depth imaging via 1560 nm wavelength single-photon detection," *Opt. Exp.*, vol. 21, no. 7, pp. 8904–8915, 2013.
[14] Y. Altmann, X. Ren, A. Mccarthy, G. S. Buller, and S. Mclaughlin, "Robust Bayesian target detection algorithm for depth imaging from sparse single-photon data," *IEEE Trans. Comput. Imag.*, vol. 2, no. 4, pp. 456–467, Dec. 2016.
[15] Y. Altmann, X. Ren, A. Mccarthy, G. S. Buller, and S. Mclaughlin, "Lidar waveform-based analysis of depth images constructed using sparse single-photon data," *IEEE Trans. Image Process.*, vol. 25, no. 5, pp. 1935–1946, May 2016.
[16] A. Kirmani *et al.*, "*First-Photon Imag. Sci.*, vol. 343, no. 6166, pp. 58–61, 2014.
[17] H. J. Kong, T. H. Kim, S. E. Jo, and M. S. Oh, "Smart three-dimensional imaging ladar using two Geiger-mode avalanche photodiodes," *Opt. Exp.*, vol. 19, no. 20, pp. 19323–19329, 2011.
[18] Z. Zhang, Y. Zhao, Y. Zhang, L. Wu, and J. Su, "A real-time noise filtering strategy for photon counting 3D imaging lidar," *Opt. Exp.*, vol. 21, no. 8, pp. 9247–9254, 2013.
[19] I. Rech, I. Labanca, M. Ghioni, and S. Cova, "Modified single photon counting modules for optimal timing performance," *Rev. Sci. Instrum.*, vol. 77, no. 3, p. 1524, 2006.
[20] R. E. Warburton *et al.*, "Enhanced performance photon-counting time-of-flight sensor," *Opt. Exp.*, vol. 15, no. 2, pp. 423–429, 2007.
[21] M. S. Oh, H. J. Kong, T. H. Kim, K. H. Hong, and B. W. Kim, "Reduction of range walk error in direct detection laser radar using a Geiger mode avalanche photodiode," *Opt. Commun.*, vol. 283, no. 2, pp. 304–308, 2010.
[22] L. Xu, Y. Zhang, Y. Zhang, C. Yang, X. Yang, and Y. Zhao, "Restraint of range walk error in a Geiger-mode avalanche photodiode lidar to acquire high-precision depth and intensity information," *Appl. Opt.*, vol. 55, no. 7, pp. 1683–1687, 2016.
[23] W. He, B. Sima, Y. Chen, H. Dai, Q. Chen, and G. Gu, "A correction method for range walk error in photon counting 3D imaging LIDAR," *Opt. Commun.*, vol. 308, pp. 211–217, 2013.
[24] F. Wang, Y. Zhao, Y. Zhang, and X. Sun, "Range accuracy limitation of pulse ranging systems based on Geiger mode single-photon detectors," *Appl. Opt.*, vol. 49, no. 29, pp. 5561–5566, 2010.
[25] A. V. Jelalian, *Laser Radar Systems*. Norwood, MA , USA: Artech House, 1992.